J Mater Sci (2011) 46:7776–7783
DOI 10.1007/s10853-011-5757-4

Electronic properties of polyvinylpyrrolidone at the zinc oxide nanoparticle surface

PVP in ZnO dispersions and nanoparticulate ZnO thin films for thin film transistors

Simon Bubel · Norman Mechau · Roland Schmechel

Received: 17 May 2011 / Accepted: 29 June 2011 / Published online: 12 July 2011

Abstract We investigated the electrical effects of polyvinylpyrrolidone (PVP), used as a dispersion agent in zinc oxide (ZnO) nanodispersions. We found PVP reduces the high surface conductivity and atmospheric sensitivity. Compared with polymer free ZnO thin films, the nanoparticulate layers with PVP exhibit a smaller density of thermally active charge carriers, a reduced density of trap states, and a Fermi level shift toward the valence band, yielding improved performance, vanishing hysteresis characteristics and reduced atmospheric sensitivity in thin film transistors (TFT). In addition, we discuss the attachment of PVP to the ZnO surface.

Introduction

Electronic functionality already enables many applications in modern consumer products like radio frequency identification tags, authentication certificates, or environmental conditions tracking. However, using the benefits of printable electronics, actual functionality as well as completely new application areas can be accessed at expected lower costs and improved eco friendliness. As a printable n-type semiconductor, particularly zinc oxide (ZnO) and related compounds such as indium gallium zinc oxide (IGZO) are widely investigated due to several advantages. ZnO is abundantly available, environmentally harmless and nontoxic. It is a transparent intrinsic n-type semiconductor with high electron mobilities [1]. Additionally, many methods of chemical synthesis are available to obtain a large variety of nano crystal morphologies and amorphous films, like zinc acetate precursor solutions [2, 3] or ammonia-based precursors [4, 5].

Besides easy processability of the ZnO semiconductor and its high electron mobility, the manipulation of the electronic states in ZnO is an important task, necessary to realize rectifying contacts and homojunctions but also to improve its aging properties. Aside from doping experiments (comprehensive review by Janotti and Van de Walle [6]), most frequently, the density of intrinsic donor states in ZnO has been controlled via the processing parameters like temperature and environmental atmosphere [7, 8]. However, many studies, especially on crystalline ZnO, show little durability of the ZnO properties adjusted by the processing parameters only. The crucial point in sustainable electronic properties is the control over the ZnO surface properties. The ZnO surface usually is in contact with the gate dielectric layer or exposed to atmosphere. In both cases, typical atmospheric adsorbates like hydroxide or oxygen ions would alter the electronic properties of the thin film or the interface [9, 10]. In addition, the surface stoichiometry of ZnO nanostructures is suspected to change with oxygen partial pressure, and atmospheric trace gases like hydrogen even may alter the electronic states in the ZnO bulk [11].

Compared to the ZnO precursor solution process which allows for the production of amorphous or crystalline thin films, a nanoparticulate ZnO thin film, e.g., processed from a dispersion, yields a much bigger intrinsic surface and therewith enables the control of the macroscopic electronic properties of the film by surface adsorbates at the ZnO nanoparticles. In this work, we use polyvinylpyrrolidone

S. Bubel (✉) · R. Schmechel
Faculty of Engineering and Center for Nanointegration Duisburg-Essen (CeNIDE), University of Duisburg-Essen, 47057 Duisburg, Germany
e-mail: simon.bubel@uni-due.de

N. Mechau
Institute of Nanotechnology, Karlsruhe Institute of Technology, Hermann-von-Helmholtz-Platz 1, 76344 Eggenstein-Leopoldshafen, Germany

(PVP) polymer adsorbates in nanoparticulate ZnO (np-ZnO) thin films to yield pronounced surface effects and also demonstrate a way to build semiconducting thin films from nanoparticle dispersions. In contrast to other approaches, where dispersion additives have been used to improve the dispersibility solely, followed by high temperature annealing (300–500 °C) to remove the additive in the thin film [12], we use the dispersion additive in the film to manipulate the electric states of the np-ZnO. In addition, the use of dispersion additives which remain in the nanoparticulate thin film is a viable route in order to obtain low temperature processed smooth interfaces and dense layers with improved mechanical properties, e.g., as was shown for tin-doped indium oxide (ITO) nanodispersions and its corresponding nanoparticulate thin films [13].

Experimental

For the nanoparticulate ZnO thin films, dispersions from anhydrous 2-methoxyethanol (2-MeEtOH) and 10 wt% of ZnO nanoparticles AdNano VP20 (ca. 25 nm, log normal 15–50 nm [14]), Evonik Industries, were prepared. To break the agglomerates in the ZnO nanoparticle powder, 1 mL of the solvent particle suspension was treated at 200 W for 10 min in an air-cooled ultrasonic bar sonotrode, VialTweeter Hielscher Ultraschall. PVP at different molar weight, 8,000 (k17) and 58,000 (k30), Sigmar Aldrich, was added to the suspension prior to the dispersion process. Thin film preparation was done via spin coating at 3,000 rpm and subsequent annealing in ambient atmosphere at 150 °C. Aluminum electrode deposition was carried out by physical vapor deposition through a shadow mask at 1×10^{-6} mbar.

For thin film transistor (TFT) characterization and *IV*-measurements, n-doped silicon (Si:P 3×10^{17} cm^{-3}) with 200 nm of thermally grown silicon dioxide (SiO_2) as gate dielectric, Fraunhofer IPMS Dresden, and microscope slide glass cover slips in UV-quality were used, respectively. The electrode width and channel length was $W = 0.74$ cm and $L = 100$ µm.

Electrical measurements were carried out in a nitrogen-filled glove box under exclusion of ambient light and using a parameter analyzer, Keithley 4200 SCS, in combination with a probe station. For each displayed transistor parameter a TFT was build and the output- and transfer characteristics were measured in forward and backward sweep with an incremental bias delay of 100 ms/V. For scanning electron microscope (SEM) analysis a Jeol JSM 7500F and for photoluminescence (PL) measurements a Horiba FluoroLog3 spectrofluorometer was used. The excitation wavelength was 320 nm and the slit width was 5 nm.

Results

Film morphology

For field effect devices like thin film transistors the roughness at the interface between the semiconductor and the gate dielectric should be small in order to get a high planar conductivity by accumulated charges due to a gate field [15]. Therefore, before we will discuss the electrical effects of PVP at the ZnO nanoparticle surface, some effects of the layer morphology will be demonstrated. PVP used in the dispersion, stabilizes the ZnO nanoparticles in the 2-MeEtOH solvent which is a solvent for PVP itself. Thus, the PVP prevents the re-agglomeration after the dispersion process conducted by a high energy ultrasound treatment as described in "Experimental" section. The reduction in ZnO agglomerate size in the dispersion by the use of organic surfactants has been shown by dynamic light scattering experiments in a previous work [16] and is also known from sol–gel synthesis of np-ZnO [17]. The same effect can be seen in the thin film morphology of the spin coated ZnO nanodispersions in Fig. 1. The SEM picture of a cross section of the ZnO film prepared from the 2-MeEtOH:ZnO dispersion without PVP and with 10 wt% of PVP on a Si:P-SiO_2 wafer is shown in Fig. 1a and b, respectively. Without PVP, the film exhibits a pronounced porosity and interface roughness compared to the film with PVP. Also, the film thickness in the sample without polymer additive is about 600 nm, whereas the film thickness of the sample with PVP is less than 200 nm (c.f. Fig. 1a, b).

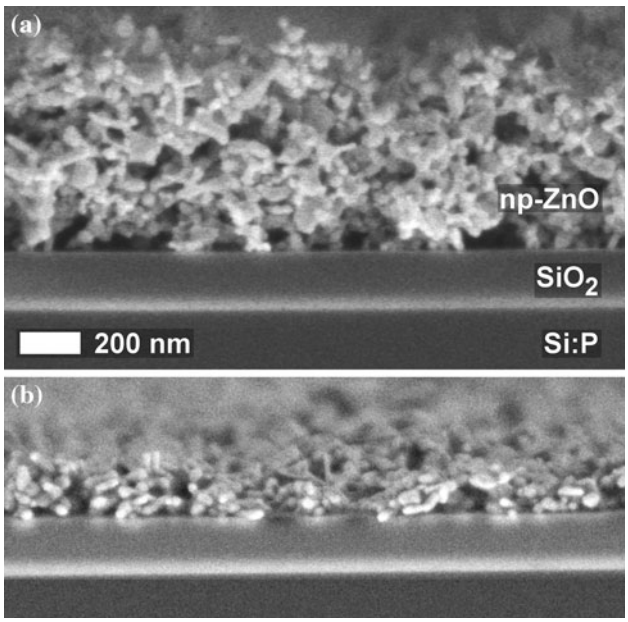

Fig. 1 Scanning electron micrograph of a nanoparticulate ZnO thin film. **a** Without PVP, **b** with 10 wt% of PVP k30 in the dispersion

In general, it can be stated that the film thickness scales with the size of the agglomerates in the nanodispersion, making the use of dispersion additives crucial for the thin film morphology.

TFT performance

Figure 2a and b shows the TFT output- and transfer characteristic of np-ZnO films, demonstrating hysteresis free n-type field effect transistor behavior. Important TFT device parameters like the saturation mobility μ_{sat} and the threshold voltage V_{th}, which reflect the transistor performance, e.g., in terms of the switching speed and the voltage, necessary to follow the device characteristic after the Shockley model [18], are defined by measuring the output- and transfer characteristics. In Fig. 3, four characteristic TFT parameters are shown for np-ZnO thin films with different PVP fractions. The calculation of the saturation mobility after the characteristic in Fig. 2b follows Eq. 1.

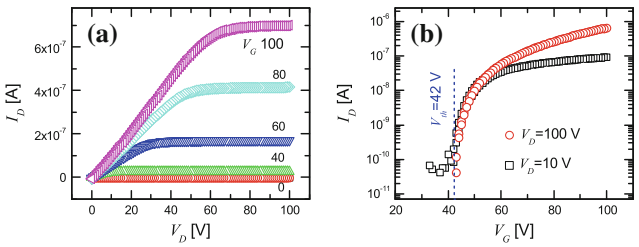

Fig. 2 TFT output (**a**) and transfer (**b**) characteristic of the np-ZnO TFT with 10 wt% PVP, annealed at 100 °C

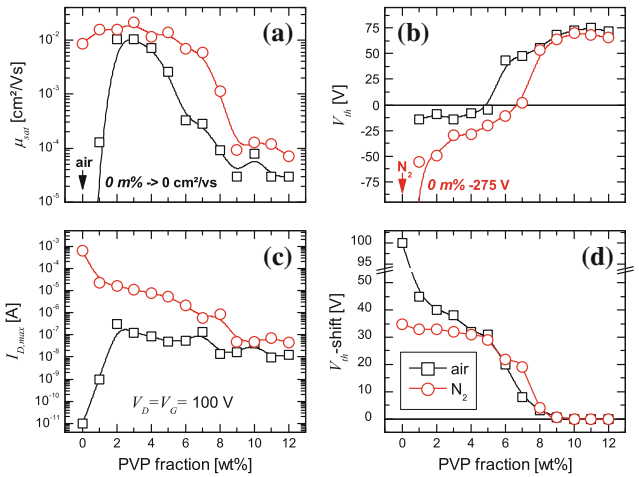

Fig. 3 From transistor characteristics derived parameters for np-ZnO TFTs produced with different PVP k30 content and measured in ambient atmosphere (*black squares*) and in nitrogen atmosphere (*red circles*). **a** Saturation mobility, **b** threshold voltage, **c** maximum drain current at $V_D = V_G = 100$ V, and **d** threshold voltage shift of the *IV*-hysteresis

$$\mu_{sat} = \left(\frac{\delta\sqrt{I_D}}{\delta V_G}\right)^2 \cdot \frac{2L}{WC_i} \quad (1)$$

I_D and V_G are the drain–source current and the gate voltage, respectively, and L and W the electrodes geometry. The sheet capacitance C_i corresponds to the thickness and permittivity of the gate dielectric, which in our case is 17.26 nF/cm^2. In Fig. 3a, μ_{sat} for air and nitrogen atmosphere is plotted against the PVP content with respect to the net weight of np-ZnO. For increasing PVP content μ_{sat} increases up to a local maximum at about 3 wt% and decreases from there on. By adding PVP into the nanodispersion, the film has a smaller porosity and increasing interface smoothness (c.f. Fig. 1) which enables improved charge transfer in the accumulation layer of the TFT. However, if the PVP content exceeds a certain threshold, the nanoparticles in the thin film become isolated from each other, as PVP is an electric insulator and hinders direct particle–particle contacts. Consequently, a decrease in μ_{sat} for higher PVP fractions can be observed.

Looking at the threshold voltage in Fig. 3b, a transition of V_{th} from the negative to the positive regime with increasing PVP content can be observed. For Ohmic source and drain contacts, which can be assumed for aluminum on ZnO, V_{th} is manly dependent on the density of thermally active charge carriers and trap states in the semiconductor [19]. In the case of np-ZnO, electrons are the majority carriers. The mobility of holes and therewith the contribution of the minority carriers, can be neglected. Hence, in TFT operation, negative charge carriers will be accumulated at a positive gate field, causing the channel conductivity to increase. In the case of a negative V_{th} the channel is conductive at $V_G = 0$ V already and a negative gate voltage is required in order to deplete the transistor channel. From Fig. 3b and c it can be seen that the intrinsic conductivity of the np-ZnO layer declines with increasing PVP content. Notably, for N_2 atmosphere and no or small fractions of PVP, the layer conductivity is exceedingly high compared to its conductivity in ambient air. Also, the mobility of the layers in air and less than 2 wt% PVP approaches zero (c.f. Fig. 3a), indicating a very poor conductivity of those np-ZnO layers in ambient atmosphere which is likewise reflected in the low maximum drain current displayed in Fig. 3c.

An explanation for the discrepancy in the characteristics in Fig. 3 at low PVP fractions and different atmospheres, can be found in the hysteresis of the transfer characteristic. Extracting the V_{th} from the forward and backward sweep of the transfer *IV*-curves and taking the difference of the two values, yields the threshold voltage shift, which is plotted in Fig. 3d. If the PVP fraction approaches 8 wt%, the V_{th}-shift becomes zero and the transistor characteristics free of hysteresis, as shown in Fig. 2. The occurrence of

hysteresis in np-ZnO TFTs has been discussed in a previous publication [20] and was found to originate from slow trap and release mechanisms induced by atmospheric or polymer adsorbates at the ZnO surface. Obviously, the only polymer adsorbate present in the thin film is PVP, which does not contribute to the hysteresis as the V_{th}-shift becomes smaller for increasing PVP fractions. This behavior is completely different from what has previously been discussed for polymer adsorbates like poly(methyl vinyl ether-alt-maleic anhydride) derivatives [20]. If PVP does not contribute to the hysteresis, its cause can be found in the atmospheric adsorbates like OH^- and O_2^-, which are known to contribute to a variety of deep and shallow acceptor like trap states [21, 22]. What can be seen in all charts in Fig. 3 is the convergence of the air and N_2 characteristics for increasing PVP fraction, indicating that the films with more PVP content are less sensitive to the surrounding atmosphere, with respect to the derived parameters μ_{sat}, V_{th}, $I_{D,max}$, and V_{th}-shift. Obviously, the application of PVP in the thin film not only improves the layer morphology but also reduces the atmospheric sensitivity and the hysteresis behavior, which are basic requirements for printable semiconductors.

Impact on the electronic states

To investigate the electronic effects of PVP at the ZnO surface, we will discuss the difference between atmospheric and PVP adsorbates in terms of the density of trap states (trap-DOS). Therefore, we will demonstrate Fermi level pinning, space charge-limited current (SCLC), and photoluminescence (PV) measurements.

The Fermi level

Diode *IV*-characteristics are recorded from Al (cathode) and Au (anode) electrodes on ZnO layers deposited on glass substrates, as shown in the microscope image in Fig. 4a. The diode characteristics exhibit strong Fermi level pinning and superposition with SCLC behavior at higher voltages. To calculate the injection barrier height from the diode reverse direction (see Fig. 4b), we will apply the mean-field approach to model the *IV*-characteristic as proposed by Neumann et al. [23]. This model is a good approximation for the measured *IV*-characteristics because it reflects the linear behavior at low voltages by diffusive charge-carrier transport and considers the space charges at the metal semiconductor interface by including the injection of charges in a limited density of states, which disturb the build up of a distinguishable thermionic emission characteristic. The applicability of the mean-field approach in comparison with a single particle model like the thermionic emission is shown by Genenko et al. [24].

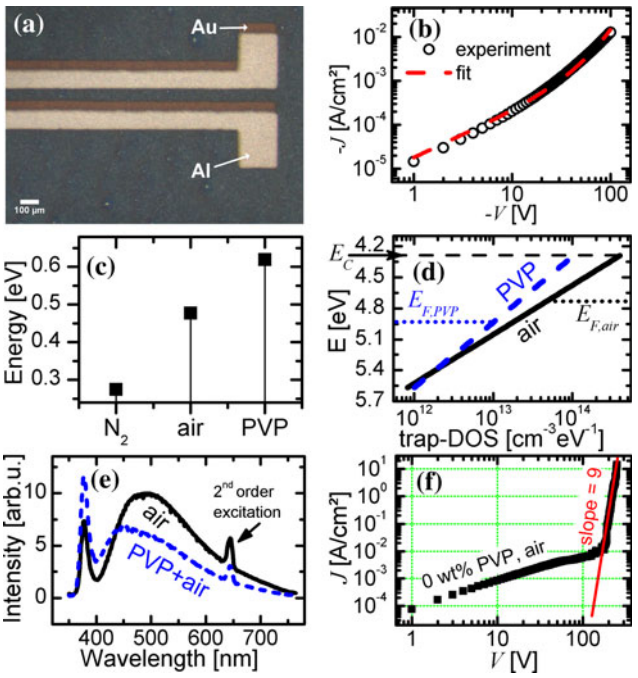

Fig. 4 **a** Microscope image of the np-ZnO thin film with Au and Al line electrodes, **b** *IV*-characteristic of the np-ZnO Diode with 10 wt% PVP, **c** injection barrier height of Aulnp-ZnO with different adsorbates, calculated for zero field, **d** trap-DOS calculated from SCLC characteristics with E_C the lower edge of the conduction band and $E_{F,PVP}$, $E_{F,air}$ the positions of the pinned Fermi energies, **e** PL spectra of np-ZnO in air with 0 and 8 wt% PVP, **f** *IV*-characteristic of the SCLC

$$J = -e\mu\frac{V+V_{Bi}}{L_{eff}}N\exp\left\{-\frac{\Delta}{kT}+\frac{e\varepsilon_s l_{TF}V}{\varepsilon_c kTL}\right\} \times\left(\exp\left\{\frac{-eV}{kT}\right\}-1\right)/\left(\exp\left\{-\frac{eL(V+V_{Bi})}{kTL_{eff}}\right\}-1\right) \quad \text{with } L_{eff}=L+\varepsilon_s\left(l_{TF}^{-}+l_{TF}^{+}\right)\simeq L+\varepsilon_s 2l_{TF} \tag{2}$$

In Eq. 2, J is the current density through the diode and V the applied bias voltage. $N \approx 10^{19}$ cm^{-3} (estim. $N \approx N_C$, vide infra Eq. 5), e, k, and $T = 300$ K are the effective total density of states, the elementary charge, the Boltzmann constant, and the ambient temperature. Δ, V_{Bi}, and $\mu \approx 10^{-2}$ cm^2/Vs denote the injection barrier height at zero field, the build in voltage and the charge-carrier mobility (see estim. lower limit in "Impact on the electronic states" section, p. 6) and $\varepsilon_s = 8$ [25] and $\varepsilon_c \approx 30$ are the relative permittivity of the semiconductor and the injecting contact, which is the part of the electrode on the nanoparticulate layer not credited to the channel length. L_{eff} is the effective channel length, which is the channel length L extended by the Thomas–Fermi length l_{TF}^{-} and l_{TF}^{+} for the cathode and anode, describing the space charge effects in the metal contacts. Even though, the

Thomas–Fermi length in metals is typically assumed to be of a view Ångström, for the rough contact $l_{TF} = 10$ nm has shown to be a practical value.

The values for Δ obtained by the fit with Eq. 2 (c.f. Fig. 4b) are displayed in Fig. 4c. Taking the work function of gold to be 5.1 eV [26] and the ZnO electron affinity to be 4.29 eV [27, 28], Δ is expected to be around 810 meV for the not compensated semiconductor. Looking at the calculated barriers in Fig. 4c, Δ is closest to the expected range for ZnO with PVP, namely $\Delta = 620$ meV. In the case of atmospheric adsorbates (480 meV) or in nitrogen atmosphere (270 meV), the barrier height is much more smaller, indicating the Fermi level to be pinned near the conduction band due to donor compensating states. In the case of Fermi level pinning, one considers a compensated semiconductor surface in contact to the metal electrode. However, in a surface governed system like the nanoparticulate layer, we will consider the nanoparticulate bulk as determined by the locally averaged density of donor and acceptor states, given that all performed measurements only target the macroscopic properties of the thin film.

Trap distribution

In the surface-governed np-ZnO thin film, the donor compensation is not likely to be caused by a few specific energy levels but as a result of energetically distributed states within the whole band gap, e.g., an exponential distribution of acceptor states represented with Eq. 3. Here, N_t and $E_C \approx 4.29$ eV (vide supra) are the total density of uncompensated trap states and the energy of the lower edge of the conduction band, respectively.

$$\tilde{N}_t(E) = \frac{N_t}{lkT}\exp\left(\frac{E - E_C}{lkT}\right) \tag{3}$$

$$J = C \cdot V^{l+1} \tag{4}$$

To probe the assumption of an energetically distributed trap-DOS, we will have a look at the SCLC characteristic, which can be seen in Fig. 4f as a result of pure Ohmic Al electrodes (c.f. a previous publication on SCLC in np-ZnO [20]). Applying a fit with Eq. 4 to the nonlinear *IV*-behavior at higher voltages, yields the parameters *C* and *l*, which can be used to derive the distribution in Eq. 3. After the findings from Zmeskal and Nespurek et al. [29, 30], Eq. 3 can be found for a thin film with two line top electrodes using Eq. 5. Notably, the here used electrodes geometry results in a slightly different equation than commonly used for coplanar (sandwiched) electrodes, e.g., as used by Lampert and Mark [31].

$$N_t = \varepsilon_s(\mu N_C)^{1/l} \cdot \left(\frac{A}{C}\right)^{1/l} \Leftrightarrow$$

$$C = N_C \mu \left(\frac{\varepsilon_s}{N_t}\right)^{l} \cdot A \text{ with} \tag{5}$$

$$A = e^{1-l}\left(\frac{2l}{l+2}\right)^{2l+1}\frac{1}{dL^{2l}}\arctan\left(\frac{2d}{L}\right)$$

Here, $N_C = 10^{19}$ cm^{-3} [32, 33] denotes the effective density of states in the conduction band. The specific charge carrier mobility μ is a unknown parameter but its lower limit can be estimated from the maximum conductivity $\sigma \approx 0.02$ S/cm and the assumption to have approximately 10^{19} cm^{-3} mobile charge carriers, which is an estimate for the uncompensated ZnO surface [34]. The estimation of the lower limit gives $\mu \approx 10^{-2}$ cm^2/Vs. Using higher values for μ than the lower limit, yields higher trap densities if $l > 1$.

With the findings from the fit and Eq. 5, the trap-DOS for np-ZnO films with atmospheric and PVP adsorbates can be plotted, as shown in Fig. 4d. The trap-DOS shows, that there are less traps present for PVP. To get an idea of the relation between the SCLC model and the electrical measurement, the position of the Fermi energy, according to the barriers in Fig. 4c, is marked in Fig. 4d. The approximation of the trap-DOS after Eqs. 4, 3, and 5 is done in the proximity of the Fermi energy, in a span only a few 10 meV above E_F, which then is the confidence region of the trap-DOS in Fig. 4d.

Interestingly, even if the np-ZnO thin film with PVP is transferred to atmosphere, the lower density of trap states, compared to np-ZnO without PVP, seem to persist. Looking at the photoluminescence spectra for both layers in Fig. 4e, an increase of the exciton emission peak at 377 nm [17, 35] at the cost of the defect emission around 500 nm can be observed for the PVP containing np-ZnO thin film. As the green defect emission inter alia can be attributed to surface anion vacancies [36], a reduction in such vacancies would reduce the high surface conductivity of ZnO and therewith enable the application of the functionalized np-ZnO films as a nondegenerate semiconductor in enhancement mode TFTs. Otherwise, the reduction in conductivity due to atmospheric adsorbates is not caused by the reduction of the high density of surfacial donor states, but seems to originate from opposing the high donor density with a high density of compensating states, as seen in the higher trap-DOS for air in Fig. 4d. In the case of PVP adsorbates, the occurrence of less compensating *and* less donor states explains, why the Fermi level is much closer to the theoretical prediction of an ideal Schottky contact between Au an ZnO. Additionally, the electrical thin film characteristics shown in Fig. 3 implicate a

reduced atmospheric decline of the conductivity if PVP was used in the layer. This raises the question, whether PVP does hinder atmospheric adsorbates at the np-ZnO surface, or whether it acts as a getter for those. However, we cannot resolve this question with the in this work performed measurements and leave it for further research.

Discussion

Why ZnO benefits from PVP?

Where PVP adsorbs to np-ZnO?

After the presentation, how ZnO devices could be improved by the use of PVP, more insight into the electrical and chemical effects of PVP adsorbates at the np-ZnO surface will be given. Like most metal oxide semiconductors ZnO exhibits n-type conduction. Due to a variety of native point defects (e.g., vacancies, interstitials, and antisites) and impurities of atmospheric species (e.g., hydrogen), bare ZnO always possesses a high density of thermal charge carriers [6]. For ZnO single crystals grown by the pressurized-melt (PM) or seeded chemical vapor transport (SCVT) technique, the carrier concentration at room temperature is about 10^{17} cm^{-3} [34]. However, at the ZnO crystalline surface and the zinc terminated surface (0001) perpendicular to the *c*-axis in particular, the concentration of donor like defects has been reported to be in the range of 10^{18} to 10^{19} cm^{-3} [37], whereas the charge-carrier concentration in the first few nanometers has been reported to be higher than 10^{19} cm^{-3} [34]. Hence, the conductivity of ZnO is strongly affected by the surface. Especially for ZnO films with a high intrinsic surface, like films of ZnO nanostructures (nanorods, -belts, -flakes, -particles) and highly porous films, the surface conductivity is able to determine the ZnO bulk properties. As atmospheric adsorbates are able to decrease or increase the surface conductivity, ZnO with high intrinsic surface is used in gas sensing devices [10, 38] (NO_2 [39], NH_3 [40], NH_4 and CO [41], H_2 [42], H_2O [9], O_3 [43], H_2S [44], and C_2H_5OH [45]).

Albeit the use of ZnO in gas sensors, the atmospheric sensitivity of the ZnO surface corrupts the electrical stability of other devices like TFTs in terms of low conductivity or large hysteresis behavior [20]. Even in the absence of atmospheric adsorbates, the high density of thermally active charge carriers would not allow np-ZnO films to be used, e.g., in naturally off TFTs (enhancement mode TFTs) or piezo-electric devices [46]. PVP adsorbed at the ZnO surface seems to be a viable route to prevent atmospheric adsorbates and simultaneously decrease the high surface conductivity. Unfortunately, due to the insulating properties of PVP in nanoparticulate films, the TFT performance decreases if too much PVP is located between the ZnO particles. But why does it work in the first place? The reason can be found in the special adsorption property of PVP at the different facets of the ZnO crystal. Zhang et al. studied the directed ZnO crystal growth in the presence of PVP k30 [47]. They found pronounced crystal growth of the nonpolar $(01\bar{1}0)$ side facets, in direction of the crystal *a*-axis, little growth of the oxygen rich $(000\bar{1})$ facet, but almost no growth of the zinc rich (0001) surface, in direction of the *c*-axis. From the growth experiments, it can be concluded that the PVP primarily adsorbs on the (0001) surface which most likely gives the biggest contribution to the surface conductivity. However, the assignability of the studies on crystalline ZnO might not be 100 % valid for np-ZnO with less distinct faceting. Owing to the selective adsorption of PVP, the benefits of PVP in the np-ZnO layer take place while still uncapped ZnO nanoparticle surfaces are available to form perculation pathways through the nanoparticulate thin film.

How PVP adsorbes to np-ZnO?

In literature, only assumptions of the PVP interaction with the ZnO surface can be found. E.g., Guo et al. [17] proposed the free Zn valences to interact with the PVP carbonyl group, whereas Jetson et al. do not exclude a possible interaction with the nitrogen in PVP [35]. However, using Fourier transform infrared spectroscopy (FTIR), we have not been able to detect any significant signal from a possible binding group. The fraction of the binding group seems to be too small compared to the unbound monomer blocks of the PVP molecule.

In Fig. 5 μ_{sat}, the on/off ratio, V_{th}, and the V_{th}-shift are plotted against the weight fraction of PVP in the np-ZnO thin film transistor for two different molecule sizes of PVP, k17 and k30, respectively. In all parameters, a similar devolution for PVP k17 and k30, shifted by about 6 wt%, can be seen. Plotting the same TFT parameters against the number of PVP molecules (mol) per mass of np-ZnO (kg) in Fig. 6, a convergence of the features in the characteristics can be seen. Considering the broad distribution of the PVP molecule lengths in the two PVP batches k17 and k30, one expects only a small significance of the presented data. Nonetheless, a valid interpretation would be, that there is only a certain amount of binding places per PVP molecule. As the end groups of the PVP molecule exhibit the highest local dipole, it can be assumed, that the main effects of PVP interaction with the zinc rich (0001) surface of ZnO originate from the molecule ends. The (0001) surface in its unsaturated state, has a positive net charge caused by the zinc cations Zn^+. The *N*-propyl-pyrrolidone of the PVP end-monomer, exhibits a dipole with its negative net

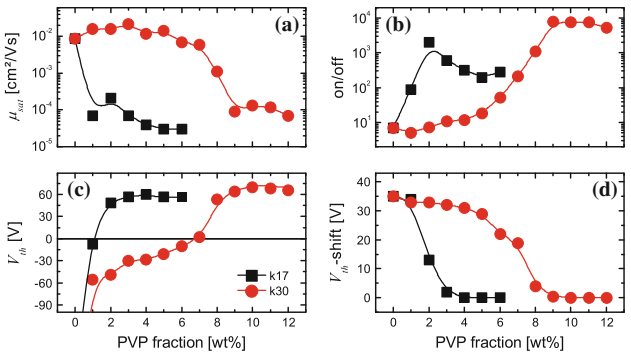

Fig. 5 Transistor parameters for different weight percent of PVP k17 and PVP k30. **a** Saturation mobility, **b** on/off ratio, **c** threshold voltage, and **d** threshold voltage shift

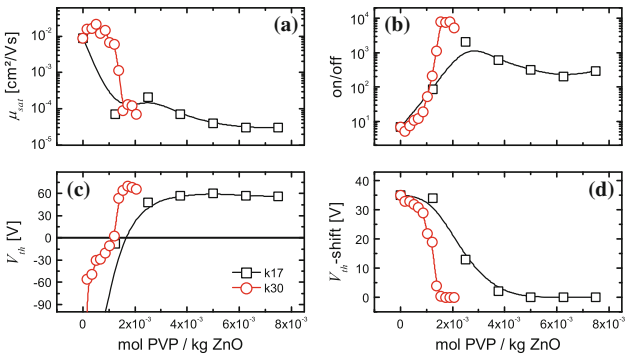

Fig. 6 Transistor parameters for different mol fractions of PVP k17 and PVP k30 per mass of np-ZnO. **a** Saturation mobility, **b** on/off ratio, **c** threshold voltage, and **d** threshold voltage shift

charge at the carbonyl group, most likely yielding the oxygen ($\delta-$) attaching to the Zn^+ site of the ZnO (0001) facet. However, in the PVP backbone the carbonyl groups are unlike harder to access and the interaction with the ZnO can be assumed to be sterically hindered, at least in the straight parts of the not bended polymer. Bringing to mind the highly speculative nature of this conclusion, additional experiments have been realized and will be published in another paper. In this experiments, we used n-type organic molecules bearing *N*-propyl-pyrrolidone linker groups. The found adsorption and electrical properties of such molecules at the ZnO surface, draw a consistent picture of the properties of the PVP end-group.

Conclusion

It has been shown that the application of PVP as a dispersing agent in ZnO nanodispersions is crucial for small agglomerates and dense and thin nanoparticulate layers with a smooth interface to the substrate or gate dielectric. As we did not try to remove the PVP from the thin film, we found positive electric effects of the PVP adsorbed to the ZnO particle surface. Without PVP, the np-ZnO films exhibit a pronounced atmospheric sensitivity and disruptive conductivity, originating from the highly conductive ZnO surface in the surface-governed nanoparticulate layers, and from the zinc rich (0001) facet in particular. From TFT, diode, SCLC, and PL measurements, we deduced the electrical effects of PVP to be caused by the selective adsorption of PVP to the zinc rich np-ZnO surface. After PVP adsorption we detected a lower density of thermally active charge carriers, accompanied by a lower density of trap states in the band gap in proximity of the Fermi level, yielding vanishing hysteresis in TFT characteristics. In contrast to the effects of PVP adsorbates, we found atmospheric adsorbates to be responsible for a high density of donor compensating states impinging upon TFT performance and reliability. However, the electrical impact of atmosphere on the TFT performance is significantly reduced if PVP is adsorbed to the ZnO surface. Additionally, we analyzed the influence of the PVP molecule length on the TFT device characteristics and found the TFT parameters to be almost independent of the molecule length, suggesting a pronounced influence of the polar PVP ends.

Looking at the insulating properties of PVP between the nanoparticles in a nanoparticulate layer, the main findings in this paper will be useful to improve surface treatments on amorphous or crystalline ZnO thin films. If the PVP end-monomer is mainly responsible for the positive electric effects like surfacial defect state reduction and atmospheric insensitiveness, a single pyrrolidone group could be useful as a linking agent in metal oxide–organic heterojunctions and self assembled monomers (SAM) to complement the conventionally [48] used carbon- and phosphonic acid linkers or to improve the charge transport in ZnO-dielectric interfaces, expedient for TFTs.

Acknowledgements The Dutch Polymer Institute (DPI), Netherlands is gratefully acknowledged for the financial support.

References

1. Ellmer K (2001) J Phys D 34(21):3097. doi:10.1088/0022-3727/34/21/301
2. Wang ZL (2009) Mater Sci Eng R 64(3-4):33. doi:10.1016/j.mser.2009.02.001
3. Tellier J, Kuscer D, Malic B, Cilensek J, Skarabot M, Kovac J, Goncalves G, Musevic I, Kosec M (2010) Thin Solid Films 518(18):5134. doi:10.1016/j.tsf.2010.03.010
4. Meyers ST, Anderson JT, Hung CM, Thompson J, Wager JF, Keszler DA (2008) J Am Chem Soc 130(51):17603. doi:10.1021/ja808243k
5. Theissmann R, Bubel S, Sanlialp M, Busch C, Schierning G, Schmechel R (2011) Thin Solid Films 519:5623. doi:10.1016/j.tsf.2011.02.073

6. Janotti A, Van de Walle CG (2009) Rep Prog Phys 72(12):126501. doi:10.1088/0034-4885/72/12/126501
7. O'Brien S, Nolan MG, Copuroglu M, Hamilton JA, Povey I, Pereira L, Martins R, Fortunato E, Pemble M (2010) Thin Solid Films 518(16):4515. doi:10.1016/j.tsf.2009.12.020
8. Kajikawa Y (2006) J Cryst Growth 289(1):387. doi:10.1016/j.jcrysgro.2005.11.089
9. Wang XH, Ding YF, Zhang J, Zhu ZQ, You SZ, Chen SQ, Zhu JZ (2006) Sensors Actuators B 115(1):421. doi:10.1016/j.snb.2005.10.005
10. Chaabouni F, Abaab M, Rezig B (2004) Sensors Actuators B 100(1-2):200. doi:10.1016/j.snb.2003.12.059
11. McCluskey MD, Jokela SJ (2007) Physica B Condens Matter 401:355. doi:10.1016/j.physb.2007.08.186
12. Walther S, Schafer S, Jank MPM, Thiem H, Peukert W, Frey L, Ryssel H (2010) Microelectron Eng 87(11):2312. doi:10.1016/j.mee.2010.03.009
13. Koniger T, Munstedt H (2009) J Mater Sci 44(11):2736. doi:10.1007/s10853-009-3357-3
14. Mechau N, Bubel S, Nikolova D, Hahn H (2010) Physica Status Solidi A 207(7):1684. doi:10.1002/pssa.200983768
15. Okamura K, Mechau N, Nikolova D, Hahn H (2008) Appl Phys Lett 93(8):083105. doi:10.1063/1.2972121
16. Bubel S, Nikolova D, Mechau N, Hahn H (2009) J Appl Phys 105(6):064514. doi:10.1063/1.3097754
17. Guo L, Yang SH, Yang CL, Yu P, Wang JN, Ge WK, Wong GKL (2000) Chem Mater 12(8):2268. doi:10.1021/cm9907817
18. Shockley W (1952) Proc Inst Radio Eng 40(11):1365. doi:10.1109/JRPROC.1952.273964
19. Sze SM, Kwok NK (2007) Physics of semiconductor devices, 3rd edn. Wiley, New York. ISBN-13: 978-0471143239
20. Bubel S, Mechau N, Hahn H, Schmechel R (2010) J Appl Phys 108(12):124502. doi:10.1063/1.3524184
21. Li QH, Liang YX, Wan Q, Wang TH (2004) Appl Phys Lett 85(26):6389. doi:10.1063/1.1840116
22. Fan ZY, Wang DW, Chang PC, Tseng WY, Lu JG (2004) Appl Phys Lett 85(24):5923. doi:10.1063/1.1836870
23. Neumann F, Genenko YA, Melzer C, von Seggern H (2006) J Appl Phys 100(8):084511. doi:10.1063/1.2360383
24. Genenko YA, Yampolskii SV, Melzer C, Stegmaier K, von Seggern H (2010) Phys Rev B 81(12):125310. doi:10.1103/PhysRevB.81.125310
25. Ashkenov N, Mbenkum BN, Bundesmann C, Riede V, Lorenz M, Spemann D, Kaidashev EM, Kasic A, Schubert M, Grundmann M, Wagner G, Neumann H, Darakchieva V, Arwin H, Monemar B (2003) J Appl Phys 93(1):126. http://dx.doi.org/10.1063/1.1526935
26. Michaelson HB (1978) Ibm J Res Dev 22(1):72
27. Jacobi K, Zwicker G, Gutmann A (1984) Surf Sci 141(1):109
28. Sundaram KB, Khan A (1997) J Vac Sci Technol A 15(2):428
29. Zmeskal O, Nespurek S, Weiter M (2007) Chaos Solitons Fractals 34(2):143. doi:10.1016/j.chaos.2006.04.006
30. Nespurek S, Zmeskal O, Sworakowski J (2008) Thin Solid Films 516(24):8949. doi:10.1016/j.tsf.2007.11.070
31. Lampert MA, Mark P (1970) Current injection in solids. Academic Press, New York and London. ISBN-13: 978-0124353503
32. Gould RD, Rahman MS (1981) J Phys D 14(1):79. doi:10.1088/0022-3727/14/1/011
33. Mahmood FS, Gould RD, Hassan AK, Salih HM (1995) Thin Solid Films 270(1-2):376. doi:10.1016/0040-6090(95)06928-3
34. Allen MW, Swartz CH, Myers TH, Veal TD, McConville CF, Durbin SM (2010) Phys Rev B 81(7):075211. doi:10.1103/PhysRevB.81.075211
35. Jetson R, Yin K, Donovan K, Zhu ZT (2010) Mater Chem Phys 124(1):417. doi:10.1016/j.matchemphys.2010.06.058
36. Koch U, Fojtik A, Weller H, Henglein A (1985) Chem Phys Lett 122(5):507. doi:10.1016/0009-2614(85)87255-9
37. Look DC (2007) Surf Sci 601(23):5315. doi:10.1016/j.susc.2007-09.030
38. Yan WJ, Mechau N, Hahn H, Krupke R (2010) Nanotechnology 21(11):115501. doi:10.1088/0957-4484/21/11/115501
39. Cho PS, Kim KW, Lee JH (2006) J Electroceram 17(2-4):975. doi:10.1007/s10832-006-8146-7
40. Devi GS, Subrahmanyam VB, Gadkari SC, Gupta SK (2006) Analytica Chimica Acta 568(1-2):41. doi:10.1016/j.aca.2006.02.040
41. Gong H, Hu JQ, Wang JH, Ong CH, Zhu FR (2006) Sensors Actuators B 115(1):247. doi:10.1016/j.snb.2005.09.008
42. Wang HT, Kang BS, Ren F, Tien LC, Sadik PW, Norton DP, Pearton SJ, Lin J (2005) Appl Phys Lett 86(24):243503. doi:10.1063/1.1949707
43. Christoulakis S, Suchea M, Koudoumas E, Katharakis M, Katsarakis N, Kiriakidis G (2006) Appl Surf Sci 252(15):5351. doi:10.1016/j.apsusc.2005.12.071
44. Wang CH, Chu XF, Wu MW (2006) Sensors Actuators B 113(1):320. doi:10.1016/j.snb.2005.03.011
45. Bie LJ, Yan XN, Yin J, Duan YQ, Yuan ZH (2007) Sensors Actuators B 126(2):604. doi:10.1016/j.snb.2007.04.011
46. Gorla CR, Emanetoglu NW, Liang S, Mayo WE, Lu Y, Wraback M, Shen H (1999) J Appl Phys 85(5):2595. doi:10.1063/1.369577
47. Zhang JH, Liu HY, Wang ZL, Ming NB, Li ZR, Biris AS (2007) Adv Funct Mater 17(18):3897. doi:10.1002/adfm.200700734
48. Liu D, Wu W, Qiu Y, Yang S, Xiao S, Wang QQ, Ding L, Wang J (2008) Langmuir 24(9):5052. doi:10.1021/la800074f